Effect of Line Inhomogeneity on the Frequency of Passive Rb^{87} Frequency Standards

A. Risley
National Bureau of Standards
Boulder, Colorado 80303

G. Busca
Laval University
Quebec, Canada

ABSTRACT

Frequency measurements versus microwave power ($P_{\mu\lambda}$), lamp temperature (T_L), and cell temperature (T_c) have been made on a passive Rb^{87} frequency standard. The lamp and integrated cell, upon which the measurements were made, are typical of the majority of the commercial rubidium standards in the field. This is the first report of the frequency dependence upon $P_{\mu\lambda}$.

The data are discussed in terms of line inhomogeneity. A spatially varying resonant frequency of the atoms in the cell plus their relative immobility produces inhomogeneities of roughly the magnitude used in the analysis. The good qualitative fit of the calculations to our data makes us feel that this inhomogeneity is the cause of the observed dependence upon $P_{\mu\lambda}$ and T_L.

I. Background

The vast bulk of the users of frequency standards find one version or another of quartz crystal oscillator adequate for their purposes. There are applications, however, where long term stability better than $\sigma_y(2,\tau>1 \text{ month}) \simeq 3\times10^{-10}$ is required [$\sigma_y(2,\tau)$, the square root of the two-sample Allan variance, is a common and useful time-domain measure of frequency stability].[1] Atomic frequency standards are used to meet these requirements and, of the various types in use, the passive Rb gas cell is probably the most prevalent.[2] The stability for a one-month averaging time (τ=1 month) is $\simeq$ 1 to 2×10^{-11} for most commercial units.[2,3] Such a unit uses what is known as an integrated cell--a single cell which contains both the Rb^{87} "working gas" and the Rb^{85} gas which acts as an optical filter.[4] Long term stability data has been reported on other units whose filter was external to the cell.[5,6] These data yield $\sigma_y(2,\tau = 1 \text{ month}) \simeq 2$ to 4×10^{-12}.

It has been suggested that slow variations of pumping lamp intensity are, at least partly, responsible for long term instabilities in some commercial Rb standards.[6] (Those exhibiting $\sigma_y(2,\tau = 1 \text{ month}) \simeq 2$ to 4×10^{-12}). It seemed reasonable to us that variations in microwave power level might also produce long term instabilities. Implicit in the idea that fluctuation in these parameters can cause instability, is the assumption that the density of buffer gas in the cell is so high that any given Rb^{87} atom is essentially fixed in position for a duration sufficient to allow stimulated emission. This procedure allows a usable signal-to-noise ratio by making wall relaxation negligible and by significantly increasing the optical pumping efficiency.[7] Under these conditions, the resonance frequency of the atoms in one part of the cell will--if the pumping light is spectrally displaced from the desired transition--be different from that in other parts of the cell. A change in either pumping light intensity (as caused, for example, by a change in lamp temperature) or microwave power will then change the weighting of the sampling of the cell and result in a frequency change. This is a line inhomogeneity effect and it is this effect which is the main subject of this paper.

II. Experimental Results on Frequency Shift

In the work reported here we have examined frequency shift versus: microwave power ($P_{\mu\lambda}$); lamp temperature (T_L); cell temperature (T_c); and magnetic bias. Frequency measurements have been made previously versus T_L and T_c, but measurements versus $P_{\mu\lambda}$ have not been reported.[8] The effect of a uniform magnetic field on the $F = 1, m_F = 0 \rightarrow F = 2, m_F = 0$ transition is given as $\nu = \nu_o + 573\ H_o^2$. The frequency of the Rb^{87} atoms in zero field is ν_o and (when the field, H_o, is given in oersteds) the output frequency, ν, is given in hertz.[7]

The measurements were made with the system shown in Figure 1. The lamp, cell, photo detector, and the temperature servos are of commercial design and manufacture. The rest of the system is from our laboratory. The output of the cavity, to which the step-recovery diode is coupled, is a spectrally pure 6.835 GHz at a level of 2.0 mW.

Our cell contains Rb^{87} and Rb^{85} in their naturally occuring proportion and N_2 at a pressure of approximately 1.3 K Pa (10 Torr).[9] This high buffer gas pressure--in addition to inhomogeneity effects emphasized here--causes a significant frequency dependence upon T_c. We measured a fractional frequency change of 3.3×10^{-10}/° C about the nominal T_c value of 73° C. Consequently, T_c had to be well stabilized and continually monitored.

Frequency measurements were made versus T_L from about 100° C to 124° C. At the lowest value of T_L, useful precision in frequency measurements could be obtained at microwave levels from $P_{\mu\lambda max}$ to $P_{\mu\lambda max}$ -30 dB. [With the $\mu\lambda$ atten (see

Figure 1) set to zero, the maximum possible power, $P_{\mu\lambda max}$, is delivered to the cavity. A rough estimate of this power is 50 μW. The power at the input to the attenuator, however, is an accurately controlled 2 milliwatts. In the figures displaying ν_{Rb} versus $P_{\mu\lambda}$, the output power from the atten is given in terms of the power at its input.] At the highest value of T_L the range was $P_{\mu\lambda max}$ to $P_{\mu\lambda max}$ -40 dB.

Figure 2 displays frequency change versus $P_{\mu\lambda}$, at nominal values of T_c and magnetic field of ~ $3x10^{-5}$ Tesla (300 milligauss) for three values of T_L. From the point of view of frequency stability, it is important to see that there is a zero slope in the T_L = 112° C curve which corresponds to zero power shift.

It is clear that the dependence on $P_{\mu\lambda}$ is normally strong. For example, at T_L = 112° C and a P of -24 dB, a change of only 0.4 dB would produce a change in frequency of about $1x10^{-11}$. Our measurements and those of Allan and Stein[8] show that the dependence of ν_{Rb} on T_L and T_c can also be quite strong for this type of unit. But, just as for the dependence on $P_{\mu\lambda}$, insufficient information is available to conclusively decide on the importance of these parameters to the long term stability of a typical commercial unit.

In our test setup, a solenoid (consisting of two short segments of coil surrounding the cell) produces--in addition to the useful H_o field--a dc magnetic gradient along the axis of the cell. This gradient is large and it results--in combination with a high buffer gas pressure--in a line inhomogeneity that produces frequency shifts of practical consequence.

The analysis of Busca et al.[10] can be easily generalized to account for an axially varying frequency due to multiple causes: For example, for a spatially varying light shift and a magnetic gradient. From the knowledge of the geometry of the solenoid around the cell and the current which it carries, we have a rough estimate of the magnetic gradient. We cannot, however, directly measure light shift as a function of axial position because the output line, in center frequency as well as in amplitude, is a weighted mean of the response over the entire cell. Nevertheless, it seemed that the situation would be clarified if we repeated our measurements of frequency versus $P_{\mu\lambda}$ and T_L with no current in the biasing coil, i.e., no applied gradient.

Figures 3 and 4 are measurements with applied gradient and without, respectively, so that Figure 3 is a repeat of Figure 2 except that we have added one new parameter. For each value of T_L we now make measurements with and without a neutral-density optical filter of 50 percent transmission. The rationale here was that light shift depends not only on peak intensity but also on the spectral distribution of the pumping light. Using the optical filter changes only intensity and that by a known amount.

III. Interpretation of the Data

Conditions are such as to cause the resonant frequencies of the atoms to vary with axial position in the cell. A comparison of Figures 3 and 4 demonstrates a significant dependence upon the intentionally applied magnetic gradient.

To apply the theory, several other parameters need also be known. At this point, a discussion of the physical mechanisms involved will be useful.

A. Physical Mechanisms

Referring to Figure 5a, the net result of the optical pumping is to overpopulate state 2 with respect to state 1.[11] If then, microwave radiation at a frequency corresponding to the 2-1 transition is applied, the ensemble is moved back towards thermal equilibrium. When the microwave frequency $\nu_{\mu\lambda}$ is on resonance, the total light transmitted through the cell to the photo detector is somewhat smaller than if it is off resonance. If $\nu_{\mu\lambda}$ is swept through resonance, an absorption curve results, the position of whose peak defines the resonant frequency of the system. To obtain effective optical pumping, it is standard practice to use Rb^{85} as a filter.[12] Unfortunately, the filtering additionally produces a shift in the resonant frequency called the light shift, LS.[10]

Use of an integrated cell--as in the present study--further complicates the interpretation. With Rb^{85} in the cell, rather than in a separate filter, the F = 1 and F = 2 pump lines both arrive at the front of the cell with significant intensity. This means that the pumping in the front part of the cell will be inefficient and that portion of the cell will make very little contribution to the net absorption. As the light progresses down the cell the Rb^{85} atoms attenuate the F = 2 line relative to the F = 1 and the pumping efficiency increases. Figure 5b shows the overlap of the Rb^{87} pump lines with the Rb^{85} absorption lines. If the relative intensities of the two pumping lines at the front of the cell are known, then the pumping rate $\Gamma(z)$, as a function of Z (the position along the axis of the cell) can be calculated. In the unit under study, the lamp contains both Rb^{87} and Rb^{85} so that there are four emission lines rather than the two under discussion above. The densities of the Rb^{87} and Rb^{85} in the lamp have been chosen so as to significantly reduce the LS.[9] The presence of the additional pumping lines further obscures the knowledge of $\Gamma(Z)$ with the result that we are forced to assume a $\Gamma(Z)$ as well as an LS dependence.

In this unit, as in other atomic standards, a Z-directed magnetic bias is applied causing the required magnetic component of the applied microwave field to also be Z-directed. The axial distribution of this component in this and other Rb devices has a sinusoidal dependence with a maximum in the center of the cell. This means that for weak $P_{\mu\lambda}$, the major interaction, and thus the major determiner of the center frequency, comes from the center of the cell. Knowledge of the microwave field distribution plus an experimental measure of linewidth versus $P_{\mu\lambda}$ allows us to evaluate the microwave excitation $\Gamma(Z)$. Figure 6 shows linewidth versus T_L with $P_{\mu\lambda}$ as a parameter. In

addition to permitting an empirical evaluation of $\Gamma(Z)$, these data aid in choosing a $\Gamma(Z)$ for use in the calculation.

The large linewidth at large $P_{\mu\lambda}$ is due to saturation of the microwave transition. The high buffer gas density holds the Rb atoms essentially fixed in position over a duration long compared to the stimulated emission time from states 2 to 1 (see Figure 5a). This means that the atoms near the center of the cell are the first to experience microwave saturation. As $P_{\mu\lambda}$ is increased, the position in the cell corresponding to the mean frequency of response moves toward the back (photo detector) end of the cell. Figure 7 shows the maximum intensity (intensity at the peak of the absorption) versus T_L with $P_{\mu\lambda}$ as the parameter. It can be seen that the saturation effect is more pronounced at lower values of T_L (lower light intensities).

B. The Calculation

What we want to calculate is the variation of the pumping rate $\Gamma'(z)$ as a function of the frequency and intensity of the microwave signal. This dependence is described by the equation[11]

$$d\Gamma'(z) = -\sigma_1 n_2(z)\Gamma'(z)dz \qquad (1)$$

where:

$$n_2 \equiv \frac{16\,[A(\Gamma')]^2\,\Gamma'(\beta')^2}{1 + (\Omega-\Omega')^2 + 4C(\Gamma')(\beta')^2} \;;$$

$$A(\Gamma') \equiv 1/(5\Gamma' + 8) \;;$$

$$C(\Gamma') \equiv A(\Gamma')\,[(\Gamma')^2 + 9\Gamma' + 8]/(\Gamma' + 1) \;;$$

$$\Gamma' \equiv \Gamma(z)/\gamma_1 \;;$$

$$(\beta')^2 \equiv [\beta(z)]^2/\gamma_1[\gamma_2 + \Gamma(z)/2] \;;$$

γ_1 = longitudinal relaxation rate in the absence of applied fields;
γ_2 = transverse relaxation rate in the absence of applied fields;
ω is the frequency of the applied microwave field;
$\omega' \equiv \omega_o + \alpha(z)$;
ω_o is the center frequency of the Rb^{87} atoms in the absence of applied fields;
$\alpha(z)$ is the total change in resonant frequency brought about by effects such as LS and magnetic gradient;
σ_1 is a proportionality constant.

The variation in pumping light--as received at the photocell--is then obtained by integrating $d\Gamma'(Z)$ over the length of the cell:

$$\Delta\Gamma' = -\sigma_1 \int_o^L n_2(z)\Gamma(z)dz \qquad (2)$$

where L is the length of the absorption cell.

If, then, the microwave frequency is varied and the integration of eq. (2) performed for each frequency, the plot of light received at the photocell versus frequency displays an absorption dip.

Equation (2) can be evaluated for a given set of parameters if $\Gamma'(z)$ is known for those conditions. We have calculated the change in ν_{Rb} versus $P_{\mu\lambda}$ by assuming two functions for $\Gamma'(z)$. The first is to simulated the T_L = 124° C data of Figure 3 and the second to simulate the T_L = 116° C of Figure 4.

These functions are based on the assumed form

$$\Gamma(z) = \Gamma_{max}\exp\left[\frac{-(z-z_{max})^2}{\Delta^2}\,4\ln 2\right] \qquad (3)$$

where Γ_{max} is estimated from the experimental results for light broadening (Figure 6). The quantities z_{max} and Δ were picked to give the best fit to the data of Figures 3 and 4. For T_L = 124° C, z_{max} is taken equal to L; for T_L = 116° C, $z_{max} \approx L/2$.

The low value of $\Gamma(z)$ at the entrance to the cell (z = 0) represents the fact (discussed above) that the Rb^{85} atoms have not yet exerted their filtering effect. As the light progresses down the cell the Rb^{85} filtering action and the absorption due to the Rb^{87}, F = 1 transition oppose each other in determining $\Gamma(z)$. For sufficiently high T_L (or low Rb^{87} density) the increasing efficiency predominates and $\Gamma(z)$ increases all the way to the end of the cell. Otherwise, the absorption attenuates the light enough that $\Gamma(z)$ reaches a maximum part way down the cell and decreases thereafter.

Either of these assumed functions for $\Gamma(z)$ can now be inserted into equation (2) and the output of the photocell calculated. (This requires the additional approximation that the effect of the cell is merely to alter the amplitude of the pumping line and not its spectral distribution.) Figure 8 shows calculations of the peak value (resonance value) of $\Delta\Gamma'$ as a function of microwave power. The assumed $\Gamma'(z)$ for T_L = 124° C was used. The +10 dB value of $P_{\mu\lambda}$ is 10 dB greater than the maximum power available in the experiment. The experimental values (from the T_L = 124° C data of Figure 7) are shown for comparison. The fit is good. Figure 9 shows the full linewidths calculated for the same set of parameters. The data from Figure 6 (T_L = 124° C) is given for comparison. Again, the fit is rather good.

To calculate ν_{Rb} versus $P_{\mu\lambda}$ we must also assume a frequency gradient, $\alpha(z)$. The results of

such a calculation are particularly sensitive to our assumptions for $\Gamma'(z)$ and (z). We emphasize again that our purpose in displaying these calculations is to show that the observed sensitivity of ν_{Rb} to T_L and $P_{\mu\lambda}$ is due to line inhomogeneity and not to claim that $\Gamma'(z)$ and $\alpha(z)$ exactly represent the experimental situation. Figure 10 shows ν_{Rb} versus $P_{\mu\lambda}$ for four sets of parameters. The upper two curves simulate the T_L = 124° C data of Figure 3. For this calculation we have assumed $\alpha(z)$ to be due entirely to an applied magnetic gradient. The gradient is taken to be parabolic in shape, with the field maximum in the center of the cell, and with that maximum corresponding to a frequency excursion of 20 Hz. For the upper of the high light intensity curves of Figure 10 we have used the assumed $\Gamma'(z)$ for T_L = 124° C. To simulate the optical filter, the curve with crosses was calculated by reducing $\Gamma'(z)$ by half.

The T_L = 116° C data of Figure 4 is simulated by the low light intensity curves of Figure 10. For the "unfiltered" curve we have used the assumed $\Gamma'(z)$ for T_L = 116° C. $\Gamma'(z)$ was reduced by half for the other curve. For both curves we have again assumed the magnetic gradient used for the other pair, but, reversed the sign. DC magnetic field measurements show that this is not only qualitatively correct but the gradient is even larger than that due to the externally applied bias. This gradient is due to the perturbing effect upon the Earth's magnetic field of the magnetic shield surrounding the cell.

Several points are worth noting about Figure 10.

High Light Intensity

In moving from the filtered to the nonfiltered curve (for fixed $P_{\mu\lambda}$) the frequency increases. We call this effect a "position shift." It is a totally different effect from the physical light shift (which was set to zero in this calculation). By removing the filter, the pumping rate is increased throughout the cell. Because the microwave intensity maximizes in the center of the cell, the increased pumping increases the relative contribution of the atoms in the middle portion of the cell, thus shifting the center frequency of the overall response to a higher value.

These curves exhibit a negative shift with increasing $P_{\mu\lambda}$. The position shift again explains this behavior. As $P_{\mu\lambda}$ is increased the relative contribution of the back end of the cell is increased. Since the frequency of the atoms in this portion of the cell is lower than in the center, the net response moves to a lower frequency. Not shown in the figure is the expected result that, as $P_{\mu\lambda}$ is decreased to very low values, the two curves asympotically approach horizontal lines.

There is a decreasing difference between the filtered and unfiltered curves as $P_{\mu\lambda}$ is increased. This is because the cell is becoming increasingly saturated as $P_{\mu\lambda}$ is increased, and consequently the increment in the position shift becomes smaller.

Each of the effects is in qualitative agreement with the T_L = 124° C data of Figure 3.

Low Light Intensity

Because the sign of the gradient is reversed here, the same arguments explain the reversed sign of the power shift and of the apparent light shift. Note that, unlike the high light intensity curves, the sign of the apparent light shift changes sign as $P_{\mu\lambda}$ goes to its maximum value. The same arguments explain this when we recall that $\Gamma'(z)$ maximizes near the center of the cell (rather than monotonically increasing as before). Figure 4 shows that this reversal also occurs experimentally.

In summary, the qualitative agreement is good but the quantitative agreement is rather poor. Our calculations strongly indicate that the spatial variation of the magnetic bias predominates over the gradient in the physical light shift in our test setup. Nevertheless, qualitative arguments suggest that a small light shift term would improve the fit to the data. Because this term (and the magnetic term, as well) may vary significantly from unit to unit, we have chosen not to belabor the point.

V. Conclusions

Frequency measurements were made on a rubidium lamp-and-cell system that is typical of the majority of the passive rubidium frequency standards in the field. The data show that frequency shift versus $P_{\mu\lambda}$ can be a large effect. There is, however, insufficient data to determine whether variations in $P_{\mu\lambda}$ are the cause of the observed long term instability in this type of unit. The inhomogeneity model discussed here--which introduces the "position shift" concept--gives a good qualitative fit to our frequency data. This is strong indication that spatial gradients in frequency combined with a relatively motionless ensemble of atoms provide the physical mechanism behind the data.

Acknowledgements

One of us (AR) wishes to acknowledge support received from several of his NBS colleaques: H. Hellwig originally proposed the study of the dependence of ν_{Rb} upon $P_{\mu\lambda}$. D. W. Allan made several suggestions about instrumentation for frequency stability measurements. F. L. Walls and D. J. Wineland made suggestions about the design of the phase-lock loop.

This work was supported in part by contract #SMS 70105 from the Space and Missiles Systems Organization of the U.S. Air Force.

REFERENCES

1. D. W. Allan "Statistics of atomic frequency standards," Proc. IEEE, Vol. 54, pp. 221-230, Feb. 1966.

2. Claude Audoin and Jacques Vanier, "Atomic frequency standards and clocks," J. of Phys. E: Scientific Instruments, Vol. 9, pp. 697-720, 1976.
3. H. Hellwig, "A review of precision oscillators," NBS Tech. Note 662, Feb. 1975. (Also in Proc. 6th PTTI, Wash., DC, Dec. 1974, pp. 59-81.
4. E. Jechart, "A new rubidium gas cell frequency standard," Proc. 27th Ann. Symp. on Freq. Cont., pp. 387-389, 1973.
5. A. R. Chi, J. H. Roeder, S. C. Wardrip, and B. Kruger, "Long-term frequency stability measurement of rubidium gas cell frequency standards," Proc. 22nd Ann. Symp. on Freq. Cont., p. 592, 1968.
6. Darwin H. Throne, "A report on the performance characteristics of a new rubidium vapor frequency standard," Proc. 23rd Ann. Symp. on Freq. Cont., pp. 274-278, 1969.
7. P. Davidovits and R. Novick, "The optically pumped rubidium maser," Proc. IEEE, Vol. 54, pp. 155-170, Feb. 1966.
8. D. W. Allan and S. R. Stein (Private communication).
9. E. Jechart (Private communication).
10. G. Busca, M. Tetu, and J. Vanier, "Light shift and light broadening in the Rb^{87} maser," Canadian J. of Phys., Vol. 13, pp. 1379-1387, July, 1973.
11. Gilles Missout and Jacques Vanier, "Some aspects of the theory of passive rubidium frequency standards," Canadian J. of Phys., Vol. 53, pp. 1030-1043, 1975.
12. P. L. Bender, E. C. Beaty, and A. R. Chi, "Optical detection of narrow Rb^{87} hyperfine absorption lines," Phys. Rev. Letters, Vol. 1, pp. 311-313, Nov. 1958.

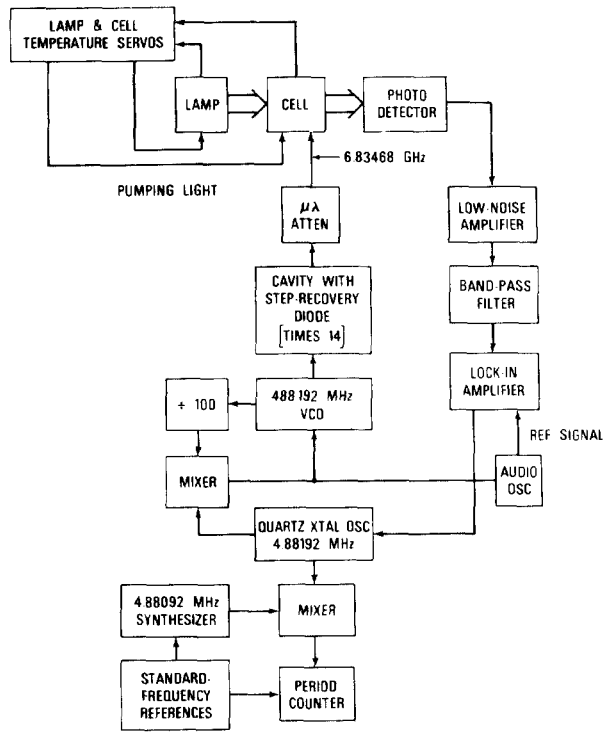

Figure 1. Block diagram of experimental setup.

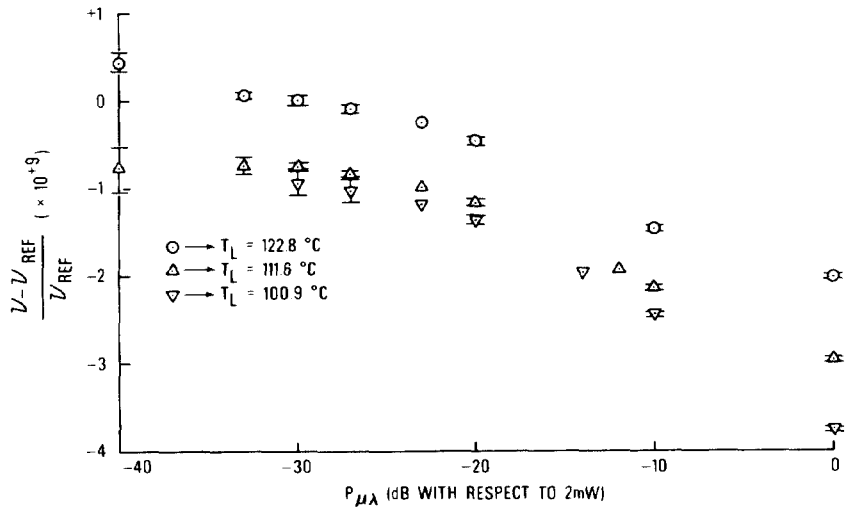

Figure 2. Fractional frequency shift (with respect to ν_{ref}) versus $P_{\mu\lambda}$. The reference frequency, ν_{ref}, is the cell frequency for T_L = 122.8° C and a $P_{\mu\lambda}$ level of -30 dB. The error bars shown in all figures are 1 sigma.

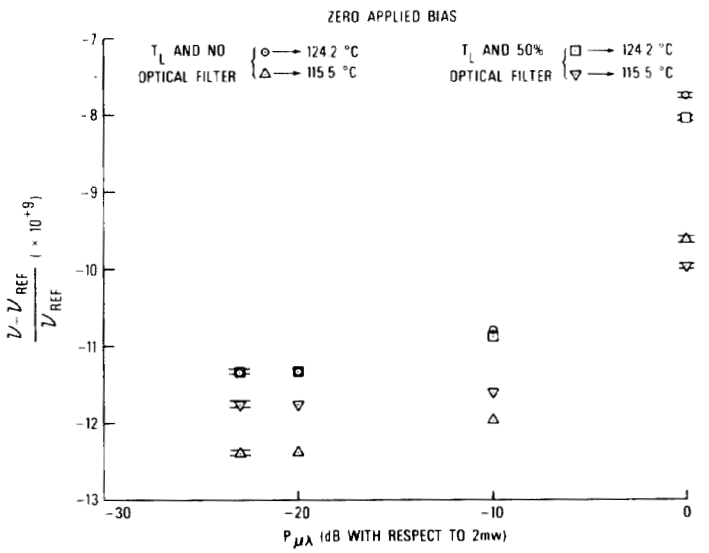

Figure 3. Fractional frequency shift versus $P_{\mu\lambda}$ with both T_L and optical filter as parameters. For each T_L, data was taken with and without the 50 percent transmission neutral-density optical filter. The standard magnetic bias applies to all data. The point at T_L = 124.2° C, with no filter, and at $P_{\mu\lambda}$ = -23 dB is, ν_{ref}.

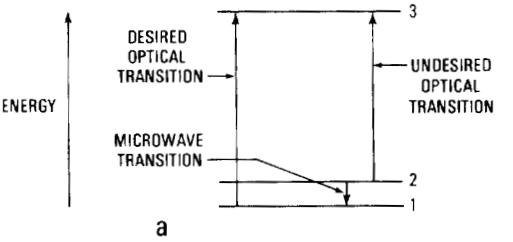

Figure 5a. Idealized three-levels system.

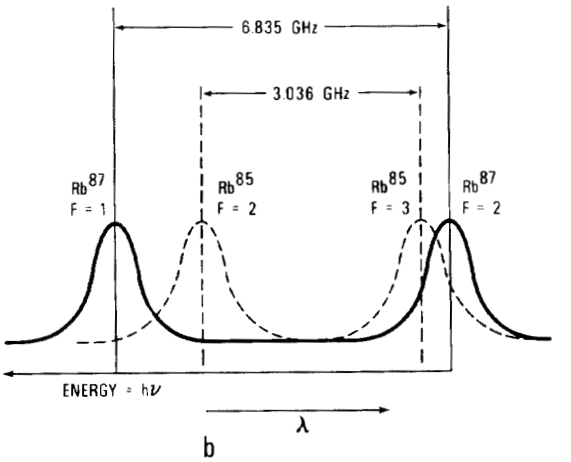

Figure 5b. The solid curves represent optical emission corresponding to the desired (F=1) and the undesired (F=2) states of Rb_{87}. The dashed curves represent absorptions corresponding to the filtering due to Rb^{85}. The strong overlap of the Rb^{87}, F=2 and the Rb^{85}, F=3 lines produces the desired filtering. The partial overlap of the Rb^{87}, F=1 and the Rb^{85}, F=2 lines lines produces an undesired true light shift.

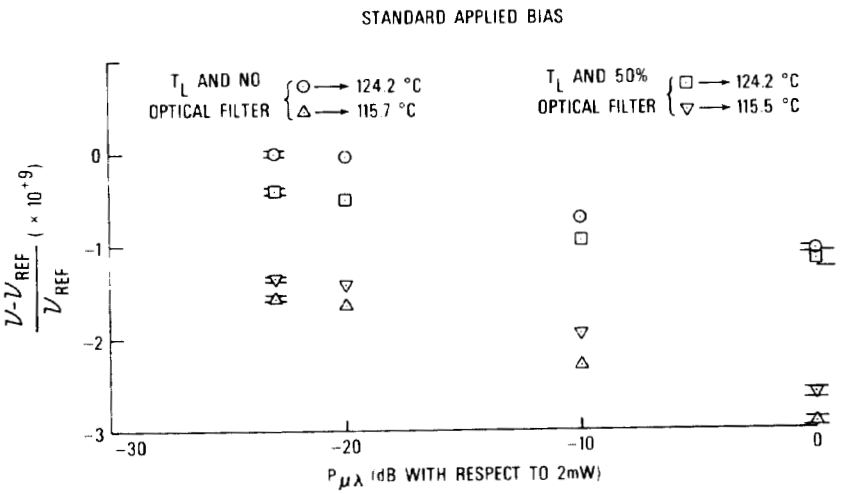

Figure 4. Same as figure 3 except that no intentional magnetic bias is applied.

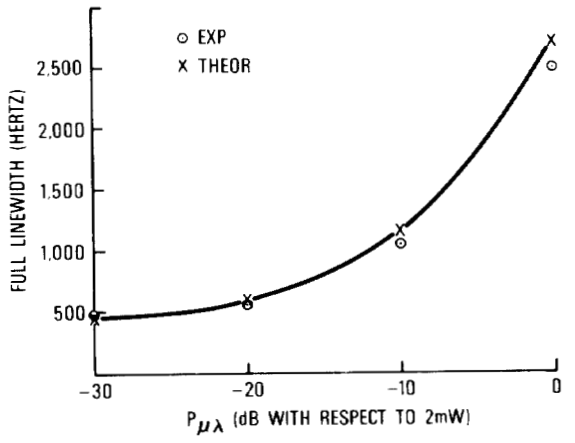

Figure 6. Full linewidth (at half power points) versus T_L. Data obtained by amplitude modulating the microwave power.

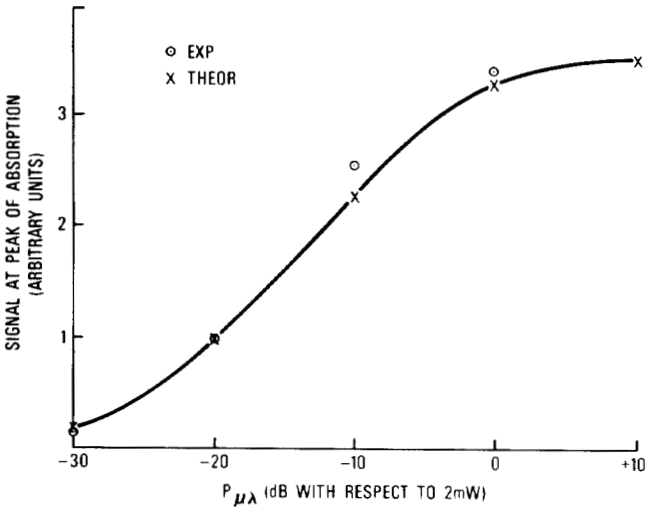

Figure 7. Peak absorption amplitude versus T_L. Data obtained by amplitude modulating the microwave power.

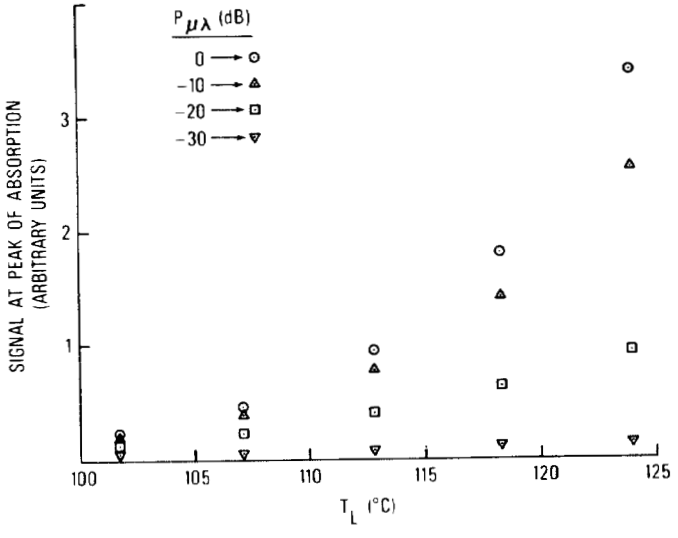

Figure 8. Theoretical prediction of peak absorption amplitude versus $P_{\mu\lambda}$. The crosses simulate data taken at T_L = 123.9° C which is shown for comparison. To emphasize saturation a theoretical point is shown for a level of $P_{\mu\lambda}$ which is 10 dB above the maximum available experimentally.

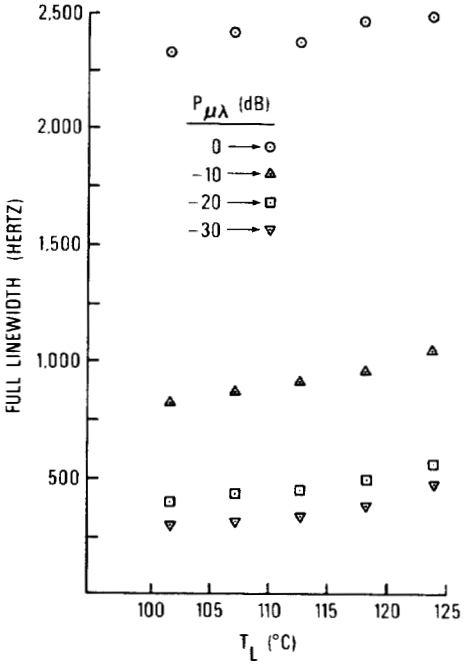

Figure 9. Theoretical prediction of full linewidth (at half power points) versus $P_{\mu\lambda}$. The crosses simulate data taken at T_L = 123.9° C which is shown for comparison.

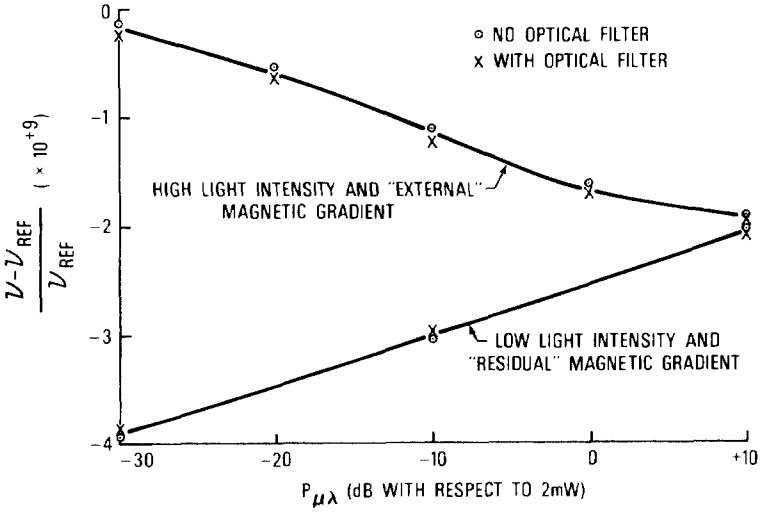

Figure 10. Theoretical prediction of fractional frequency shift versus $P_{\mu\lambda}$. The two upper curves simulate the T_L = 124.2° C data of figure 3. The lower pair of curves-- which simulate the T_L = 115.5° C data of figure 4-- were calculated from a magnetic gradient of opposite sign to that used in the upper pair of curves. In this figure, ref is arbitrary. Unlike the actual data, the average frequency offset between the upper and lower pair of curves has no meaning. It is the change versus $P_{\mu\lambda}$ and with filter which is important.